

## VCST Internal Memo

**Title:** Analysis of Preliminary FPI Measurements for JPSS-1 VIIRS

**Memo Number:** 2016\_001

**Revision:** 01

**Date:** January 15, 2016

**Author:** Jeff McIntire

**To:** Xiaoxiong Xiong and James Butler

**Cc:** Hassan Oudrari, Kwo-Fu (Vincent) Chiang, Jon Fulbright and Aisheng Wu

---

### References

- [1] BDAY.ETP-431 RC-FPI, "VISNIR / DNB Radiometric Response with FPI," Jose Parrilla, November 18, 2014.
- [2] NIST\_RC-2\_FPI\_TP\_Rev D, "Flat Plate Illuminator (FPI) Operation in Support of NPP VIIRS RC-2," September 3, 2014.
- [3] VCST\_TECH\_REPORT\_2015\_005, 'Preliminary Analysis of FPI Testing at BATC,' Jeff McIntire, March 17, 2015.
- [4] NICST\_MEMO\_11\_007, "VIIRS F1 Spacecraft Radiometric Performance Analysis (RC-2) with FPI Source," Shihyan Lee and Jeff McIntire, June 29, 2011.
- [5] VIIRS\_J1\_Prelaunch\_FPI\_Ambient\_Aero\_150317, "J1 VIIRS Pre-Launch FPI Testing at BATC in ambient Environment," David Moyer, March 17, 2015.
- [6] FPI\_DRB\_PreEnv\_20150319, "FPI Gain and SNR Analysis at Spacecraft Level,' Eric Johnson, march 19, 2015.
- [7] VCST\_TECH\_MEMO\_2015\_024, "J1 VIIRS Reflective Radiometric Response and Sensitivity (RC-2)," Jack Ji, Jeff McIntire, Hassan Oudrari, and Tom Schwarting, December 21, 2015.
- [8] "A vacuum-compatible flat plate radiometric source for system-level testing of optical sensors," S. W. Brown, A. W. Smith, J. T. Woodward, K. R. Lykke, B. Guenther, R. W. Lambeck, and R. A. Barnes, *Proc. SPIE*, **7474**, 747412, 2009.
- [9] FPI TVAC TRR 28 May 2014, "J1 VIIRS Flat Plate Illuminator (FPI) Pre Ship Review (PSR) / Test Readiness Review (TRR)," Mark Schwarz, Steve Brown, and Craig Kent, May 28, 2014.
- [10] VCST\_TECH\_MEMO\_2015\_020, "J1 VIIRS Relative Spectral Response (RSR) Measurement for the VisNIR bands from Pre-launch FP-15 and FP-16 Testing," Thomas Schwarting, Jeff McIntire, and Jack Ji, December 10, 2015.
- [11] VCST\_TECH\_REPORT\_2014\_018, "DNB Radiometric Calibration from RC1 Part 3," Tom Schwarting and Shihyan Lee, March 5, 2014.
- [12] VIIRS PRD Rev C, 'Joint Polar-orbiting Satellite System (JPSS) Visible Infrared Imaging Radiometer Suite (VIIRS) Performance Requirements Document (PRD),' Raytheon.

### 1. Introduction

After the JPSS-1 VIIRS instrument finished its sensor level environmental testing but before the instrument was shipped to the spacecraft vendor (December 2014), a radiometric performance test using the Flat Plate Illuminator (FPI) as a source was conducted in ambient conditions [1,2]. A second round of testing was conducted after the instrument was integrated into the spacecraft, also performed in ambient conditions (March 2015). Preliminary analysis of those tests were performed [3], based in large part on lessons learned during SNPP VIIRS testing [5]. Analysis was also conducted by other groups [5,6].

The goal of the testing was to verify that the gain and SNR for the bands on the warm focal planes (VisNIR bands and DNB) had not drifted significantly compared to sensor level ambient testing. The analysis contained within this memo will estimate the gains and SNR, and compare the FPI results to instrument level thermal vacuum results [7]. The test data used in this work is listed in Table 1.

## **2. FPI**

The FPI was developed by NIST to serve as a quality control check on the radiometric performance and stability of SNPP VIIRS [8,9]. The FPI used for JPSS-1 testing utilizes four sources: 3 Xe arc lamps and 1 supercontinuum. Bifurcated fiber optic bundles are used to transfer the radiant flux from the sources to a terminated fiber plate. The bundles were distributed such that output from the four sources was evenly distributed across the flat plate. A ground glass diffuser plate could also be placed in front of the flat plate (the diffuser was in place for the second test analyzed in this work). The FPI was transitioned through 11 source power levels (100, 80, 60, 45, 35, 25, 15, 10, 5, and 0 in percent). For each test configuration, the spectral radiance of each power level was measured. The different radiance levels are shown in Figure 1 for the first test run. Figures 2 and 3 show how the features in the 100 % power level match the spectral response of the sensor [10]. The spectral radiance measurements were convolved with the spectral response of the sensor to determine the spectral radiance for each of the VisNIR bands (for the DNB, the radiance was corrected by the SIS100 spectral radiance); these values are listed in Tables 2 and 3. The radiances listed in Table 3 are the average of the pre- and post-test measurements.

The FPI has the advantage that it is compact and can be placed in the thermal vacuum chamber [8,9]. However, the FPI is non-Lambertian; in addition, its radiometric stability and uniformity were not as well characterized as the integrating sphere used in instrument level testing.

## **3. VIIRS Data**

For the FPI tests, VIIRS was operated in diagnostic mode with the telescope rotating under laboratory ambient conditions [1]. The DNB as well as the cold focal planes were not cooled. Testing was performed on both electronics sides A and B; radiance data were not available for the December 2014 test on electronics side B, so no analysis of that data is performed here. For each FPI power level, the VisNIR bands were operated in both fixed high and fixed low gain. The DNB was operated in fixed aggregation modes 1 and 20 for each FPI power level.

## **4. Results (December 2014 Testing)**

The data collected during the December 2014 testing exhibited both spatial and temporal fluctuations, in contrast to the expected source profile observed in SNPP VIIRS testing [4]. Figure 4 shows an example of the source profile for 6 different scans collected by band M1 high gain (detector 6, HAM side A) at the 100 % power level. The spatial variations (the large spikes that occur approximately every 50 samples along the profile) were attributed to the non-random distribution of the fiber bundles in the fiber plate. This feature was most pronounced for detectors 1, 6, 11, and 16; it was also most pronounced at shorter wavelengths where the Xe lamps dominate, but less so at longer wavelengths where the supercontinuum source is more important. Installation of the diffuser plate smoothed out this effect in later testing. The temporal variation was attributed to the instability of the Xe arc lamps due to age; new lamps were used in later testing.

The blackbody view was used as a dark offset, and subtracted scan by scan from the Earth view data. The sample range chosen for the December 2014 test was 800 – 1099 for M bands, 1600 – 2199 for I bands, 950 – 1059 for DNB aggregation zone 1, and 1200 – 1549 for DNB aggregation zone 20. The average dn over all scans for each sample in the above ranges per collect was calculated. The dn profile for each scan in this sample range was fit to a fourth order polynomial. Two examples of this are shown in Figures 5 and 6 (upper plots), where the black line indicates the fit. The lower plots in both Figures 5 and 6 indicate the dn residual with respect to the fit. Note that the temporal variation in the profile between the two different scans was largely removed by this fit, while the spatial features remain. Taking the standard deviation over all samples in a given scan would include the spatial inhomogeneity, and the noise in the source would dominate the sensor noise. Instead, the standard deviation over scans for each particular sample was calculated; this approach attempts to isolate the sensor noise from the source noise. The SNR for each sample was then estimated from the average dn divided by the standard deviation. In this work, the SNR for each FPI power level is taken to be the average SNR over the extracted sample range; this should smooth out the effects of the spatial non-uniformity as well as residual effects of the fit.

The linear gain was then estimated by fitting the radiance to the average dn (using the middle sample). Examples of this fitting are shown in Figures 7 and 8 for bands M1 high gain and M7 high gain. Due to the sparsity of measurements for some bands, all available data with dn between 50 and 3400 was used in a linear fit for each detector, shown by the solid lines in Figures 7 and 8. Note that the vertical dashed lines indicate the specified limits of the dynamic range, and that many of the FPI levels saturate M7 high gain as seen when the radiance reaches about 40 W/cm<sup>3</sup>/sr. The band average linear gains (HAM side A) are listed in Table 4 in comparison to results from sensor level thermal vacuum testing [7]. Note that for the single gain bands, the average of the high and low gain tests are listed in the table. The percent difference between the FPI results and the SIS100 are also listed, with all VisNIR bands within 11 %. The DNB LGS gains for aggregation modes 1 and 20 were compared to Ambient level sensor testing [11] (as the DNB focal plane was not cooled); results showed the gain derived from the FPI data was up to 16 % larger. HAM side B results are not shown, but are consistent with HAM side A results.

The SNR at  $L_{TYP}$  was estimated by fitting a quadratic polynomial to the measured SNR (the function used to fit the SNR in [7] was not used here due to the sparsity of measurements). Figures 9 and 10 show the measurements along with the fits for bands M1 high gain and M7 high gain. The red vertical dashed lines indicate the limits of the dynamic range, while the blue vertical dashed line denotes  $L_{TYP}$ . The same FPI levels used in the linear gain determination were used in the SNR fitting. The band average SNR at  $L_{TYP}$  are listed in Table 6 for HAM side A and compared to the sensor level thermal vacuum results as well as the specification [12]. Bands M1 and M2 low gain measurements were below the specified dynamic range, so no value was calculated. FPI results were smaller than SIS100 results, and in general exceeded the specified limit. However, bands M2 high gain, M3 high gain, and M4 high gain did not meet the specification. HAM side B results are not shown, but are consistent with HAM side A results.

## 5. Results (March 2015 Testing)

The data collected during the March 2015 testing did not show the spatial and temporal fluctuations observed in December 2014 testing. Figure 11 shows an example of the source profile for 6 different scans collected by band M1 high gain (detector 6, HAM side A) at the 100 % power level. The spatial variations were reduced through the installation of the diffuser plate. The temporal variation attributed to the instability of the Xe arc lamps were avoided by replacing the lamps.

The data was processed in the same manner as with the December 2014 data, except that the samples ranges used were 960 – 1119 for M bands, 1920 – 2239 for I bands, 990 – 1079 for DNB aggregation zone 1, and 1400 – 1549 for DNB aggregation zone 20. Two examples of dn profile for band M1 are shown in Figures 12 and 13 (upper plots), where the black line indicates the fourth order polynomial fit. The lower plots in both Figures 12 and 13 indicate the dn residual with respect to the fit. Note that the temporal variation in the profile was largely absent, and that the spatial features are also small.

The linear gain was then estimated by fitting the radiance to the average dn (using the middle sample). Examples of this fitting are shown in Figures 14 and 15 for bands M1 high gain and M7 high gain. The linear fits for each detector are shown by the solid lines in Figures 14 and 15. Note that the vertical dashed lines indicate the specified limits of the dynamic range, and that many of the FPI levels saturate M7 high gain as seen when the radiance reaches about 40 W/cm<sup>3</sup>/sr. The band average linear gains (HAM side A) are listed in Tables 4 and 5 in comparison to results from sensor level thermal vacuum testing [7] and December 2014 FPI testing. Note that for the single gain bands, the average of the high and low gain tests are listed in the table. The percent difference between the FPI results and the SIS100 are also listed, with all VisNIR bands within 5 %. The DNB LGS gains for aggregation modes 1 and 20 were compared to Ambient level sensor testing (as the DNB focal plane was not cooled); results showed the gain derived from the FPI data was up to 10 % larger. HAM side B results are not shown, but are consistent with HAM side A results.

The SNR at L<sub>TYP</sub> was estimated by fitting a quadratic polynomial to the measured SNR. Figures 16 and 17 show the measurements along with the fits for bands M1 high gain and M7 high gain. The red vertical dashed lines indicate the limits of the dynamic range, while the blue vertical dashed line denotes L<sub>TYP</sub>. The band average SNR at L<sub>TYP</sub> are listed in Tables 6 and 7 for HAM side A and compared to the sensor level thermal vacuum results. FPI results were smaller than SIS100 results, and in general exceeded the specified limit. However, bands M2 high gain, M3 high gain, and M4 high gain did not meet the specifications. HAM side B results are not shown, but are consistent with HAM side A results.

## 6. Summary

JPSS-1 VIIRS FPI data from December 2014 and March 2015 test runs were analyzed and compared to thermal vacuum results (gains and SNR). The following is a list of findings:

- The VisNIR band average gains from December 2014 FPI testing were within 11 % of SIS100 results from TV testing. The agreement was within 5 % for the comparison between the band average VisNIR gains derived from March 2015 FPI testing and SIS100 results from TV testing.
- The SNR at L<sub>TYP</sub> was above the specification for both rounds of FPI testing for all bands except M2 high gain, M3 high gain, and M4 high gain. FPI results were lower than SIS100 results from TV testing.
- The DNB LGS gains were up to 16 % and 10 % different from the SIS100 results for the December 2014 and March 2015 FPI tests.

Table 1: FPI test data from the two test runs

Date	UAID	Collects	Electronics Side	Gain	DNB Agg Mode
December 2014	4304563	1, 3, 5, 7, 9, 11, 13, 15, 17, 19, 21	A	High	1
	4304563	2, 4, 6, 8, 10, 12, 14, 16, 18, 20, 22	A	Low	20
	4304565	1, 3, 5, 7, 9, 11, 13, 15, 17, 19, 21	B	High	1
	4304565	2, 4, 6, 8, 10, 12, 14, 16, 18, 20, 22	B	Low	20
March 2015	4304636	1, 3, 5, 7, 9, 11, 13, 15, 17, 19, 21	A	High	1
	4304636	2, 4, 6, 8, 10, 12, 14, 16, 18, 20, 22	A	Low	20
	4304638	1, 3, 5, 7, 9, 11, 13, 15, 17, 19, 21	B	High	1
	4304638	2, 4, 6, 8, 10, 12, 14, 16, 18, 20, 22	B	Low	20



Table 4: Gain comparison between SIS100 and FPI testing (HAM side A, electronics side A).

Band	Gain Mode / Agg Mode	SIS100	FPI (Dec 2014)	$\Delta$ [%]	FPI (Mar 2015)	$\Delta$ [%]
I1	SG	4.70	5.07	-7.37	4.80	-2.16
I2	SG	8.78	8.54	2.81	9.11	-3.62
M1	HG	18.3	19.6	-6.80	18.6	-1.79
M1	LG	4.27	4.60	-7.10	4.38	-2.43
M2	HG	21.1	23.3	-9.45	20.8	1.44
M2	LG	4.21	4.73	-11.0	4.24	-0.74
M3	HG	25.9	26.7	-2.85	26.1	-0.62
M3	LG	4.16	4.24	-1.78	4.19	-0.61
M4	HG	34.8	39.0	-10.8	34.4	1.12
M4	LG	4.43	4.81	-7.81	4.33	2.41
M5	HG	48.4	53.8	-10.1	50.2	-3.69
M5	LG	4.84	5.17	-6.39	4.94	-2.04
M6	SG	77.0	81.8	-5.92	77.2	-0.32
M7	HG	101	100	0.59	104	-3.28
M7	LG	8.97	8.54	5.00	9.10	-1.47
DNB LGS	1	82.9	98.7	-16.0	90.0	-7.89
DNB LGS	20	16.3	18.6	-12.4	17.8	-8.43

Table 5: Gain comparison between SIS100 and FPI testing (HAM side A, electronics side B).

Band	Gain Mode / Agg Mode	SIS100	FPI (Mar 2015)	$\Delta$ [%]
I1	SG	4.70	4.71	-0.29
I2	SG	8.78	9.18	-4.33
M1	HG	18.1	18.4	-1.60
M1	LG	4.45	4.35	2.19
M2	HG	21.0	20.6	1.72
M2	LG	4.28	4.20	1.99
M3	HG	25.9	26.1	-0.72
M3	LG	4.20	4.22	-0.55
M4	HG	34.7	34.1	1.88
M4	LG	4.43	4.28	3.46
M5	HG	48.2	49.5	-2.55
M5	LG	4.83	4.85	-0.39
M6	SG	46.9	77.3	-0.54
M7	HG	100	103	-2.51
M7	LG	8.95	9.15	-2.17
DNB LGS	1	80.1	88.5	-9.49
DNB LGS	20	15.7	17.5	-10.3

Table 6: SNR at  $L_{TYP}$  comparison between SIS100 and FPI testing (HAM side A, electronics side A).

Band	Gain Mode / Agg Mode	SIS100	FPI (Dec 2014)	FPI (Mar 2015)	Specification [12]
I1	SG	257	202	198	119
I2	SG	293	235	264	150
M1	HG	641	380	355	352
M1	LG	1130	~	~	316
M2	HG	580	347	337	380
M2	LG	1026	~	~	409
M3	HG	714	401	389	416
M3	LG	1245	522	474	414
M4	HG	567	345	325	365
M4	LG	1002	482	454	315
M5	HG	387	252	265	242
M5	LG	899	477	472	360
M6	SG	433	285	298	199
M7	HG	555	311	378	215
M7	LG	948	425	528	340

Table 7: SNR at  $L_{TYP}$  comparison between SIS100 and FPI testing (HAM side A, electronics side B).

Band	Gain Mode / Agg Mode	SIS100	FPI (Mar 2015)	Specification [12]
I1	SG	254	195	119
I2	SG	293	263	150
M1	HG	715	381	352
M1	LG	1119	~	316
M2	HG	579	347	380
M2	LG	1018	~	409
M3	HG	710	389	416
M3	LG	1242	586	414
M4	HG	567	313	365
M4	LG	977	496	315
M5	HG	381	254	242
M5	LG	913	493	360
M6	SG	435	289	199
M7	HG	556	364	215
M7	LG	931	532	340

Figure 1: Spectral radiance for the FPI across power levels for the first test run (December 2014).

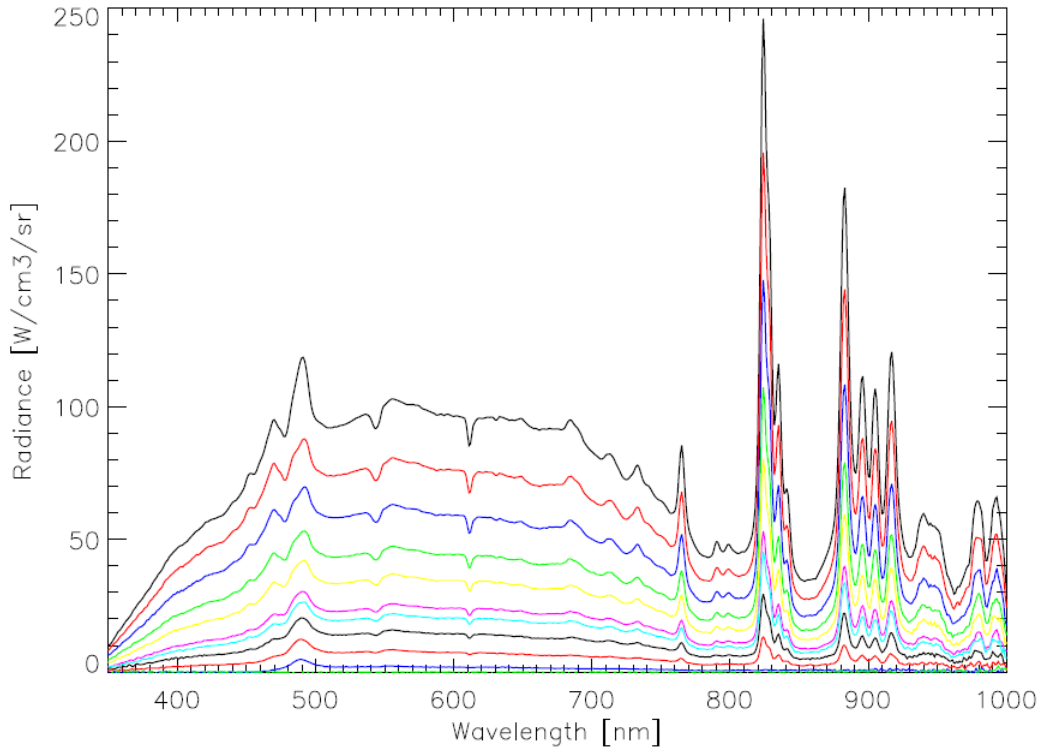


Figure 2: Spectral radiance of the FPI compared to the spectral response of VisNIR bands.

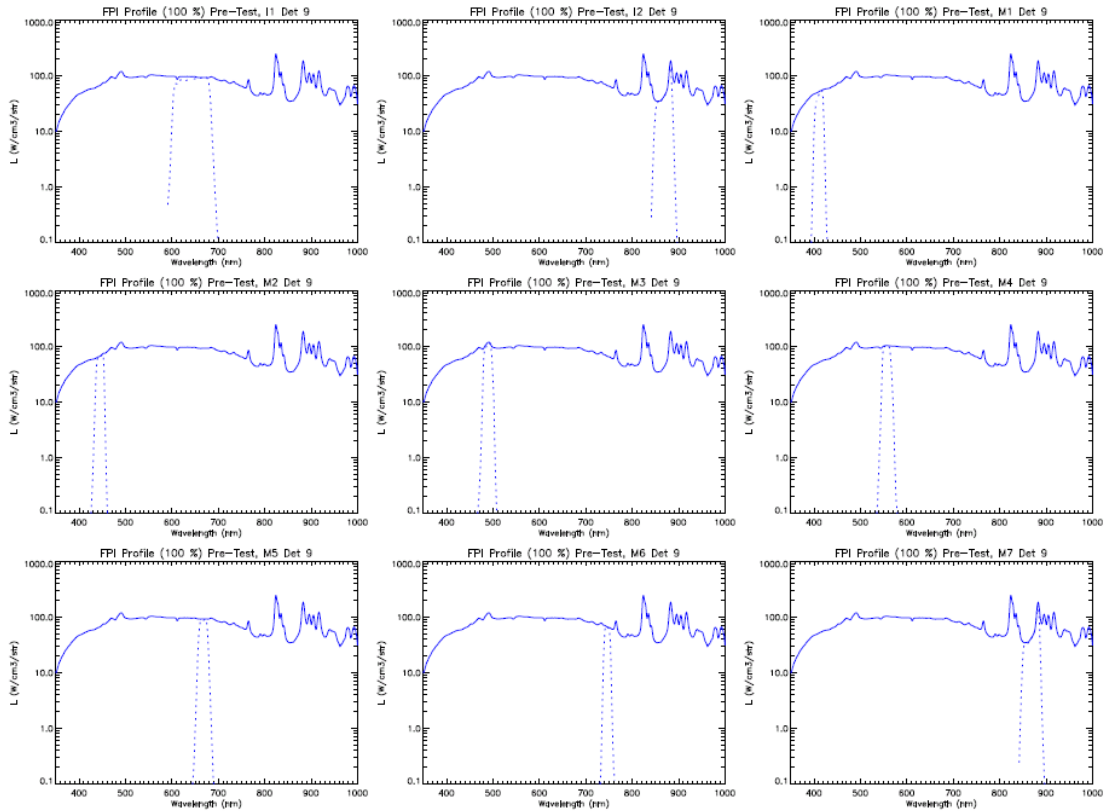


Figure 3: Spectral radiance of the FPI compared to the spectral response of the DNB.

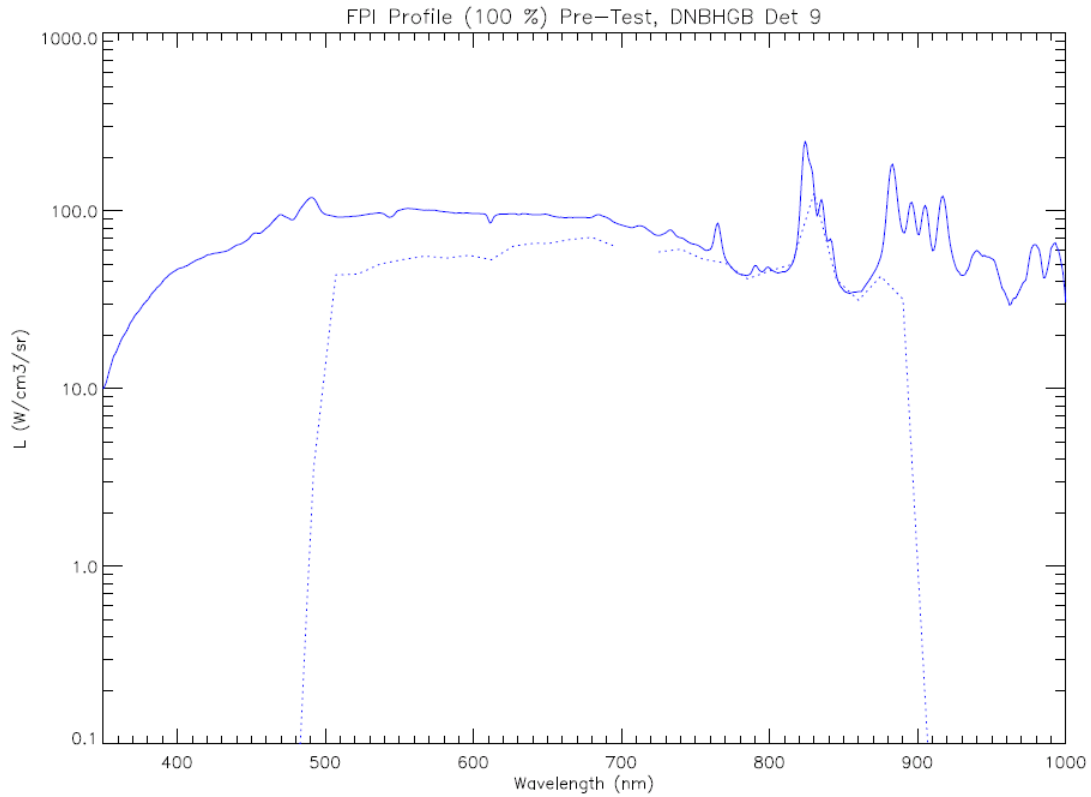


Figure 4: Example of temporal and spatial variations observed in December 2014 FPI testing. Band M1 high gain, detector 6, HAM A is shown for scans 1, 19, 39, 59, 79, and 99 (the FPI is at 100 %).

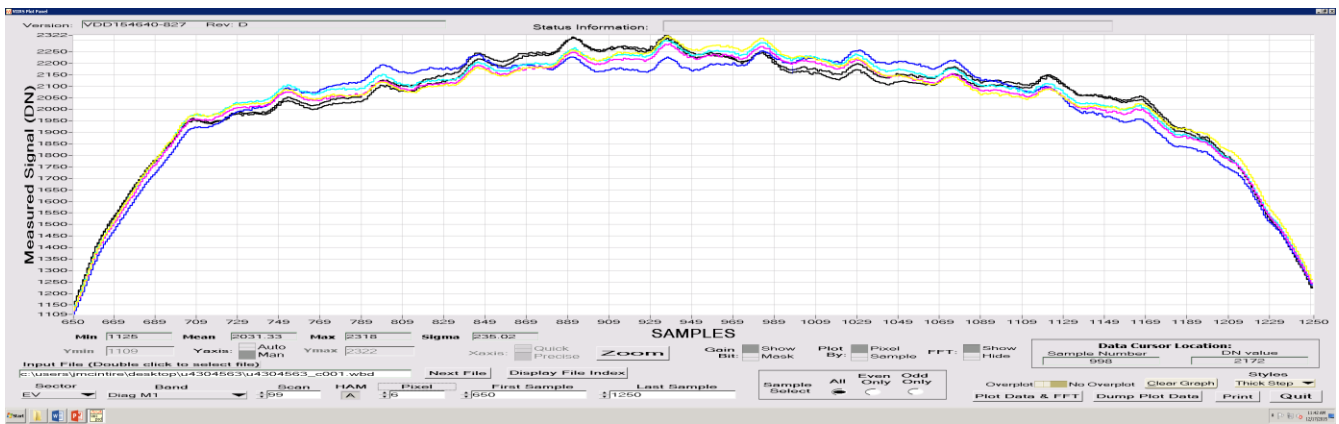


Figure 5: Band M1, scan 1 dn profile for the 100 % FPI power level with fit (upper plot) and residual to fit (lower plot), from December 2014 data.

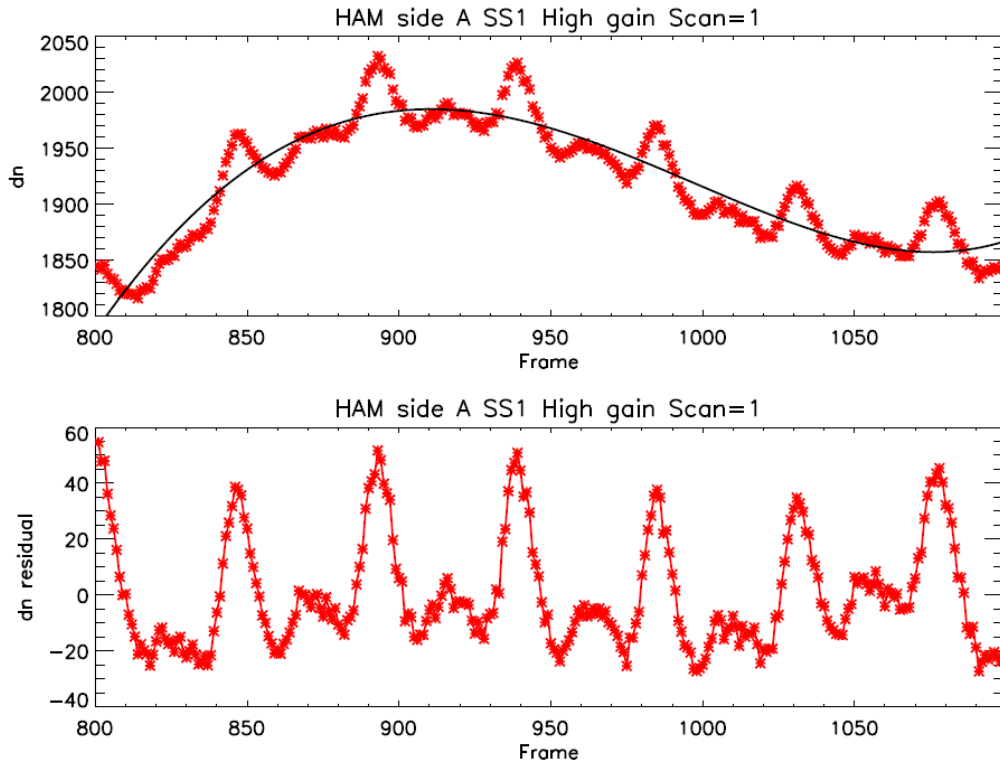


Figure 6: Band M1, scan 31 dn profile for the 100 % FPI power level with fit (upper plot) and residual to fit (lower plot), from December 2014 data.

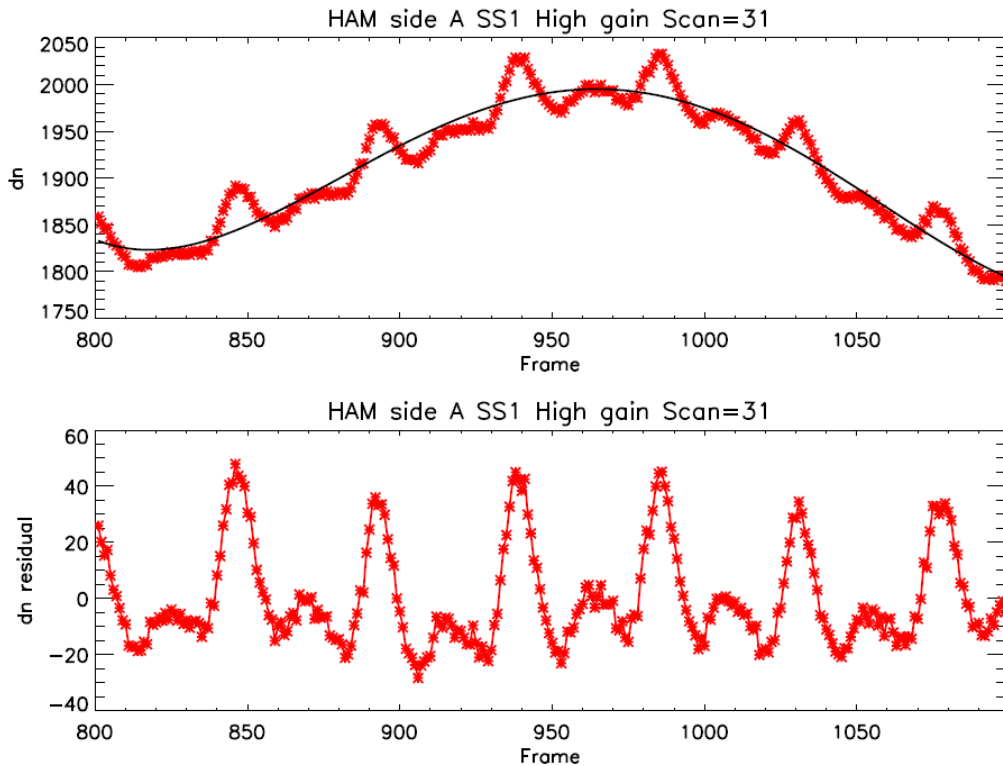


Figure 7: Fit of radiance to dn for M1 high gain, HAM side A (using December 2014 data).

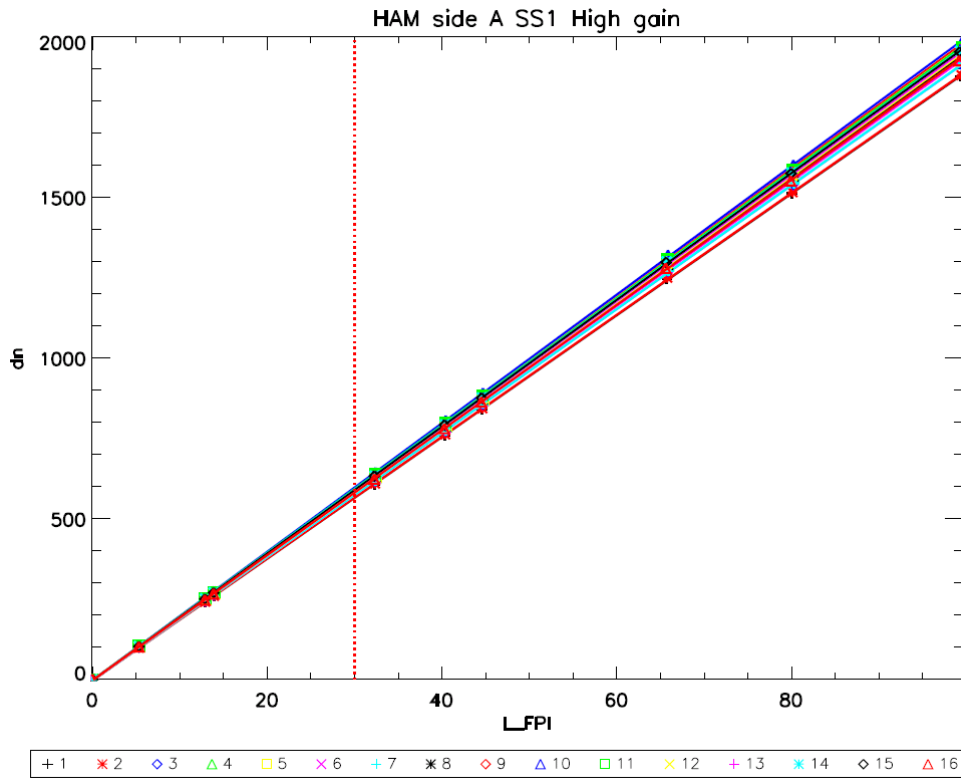


Figure 8: Fit of radiance to dn for M7 high gain, HAM side A (using December 2014 data).

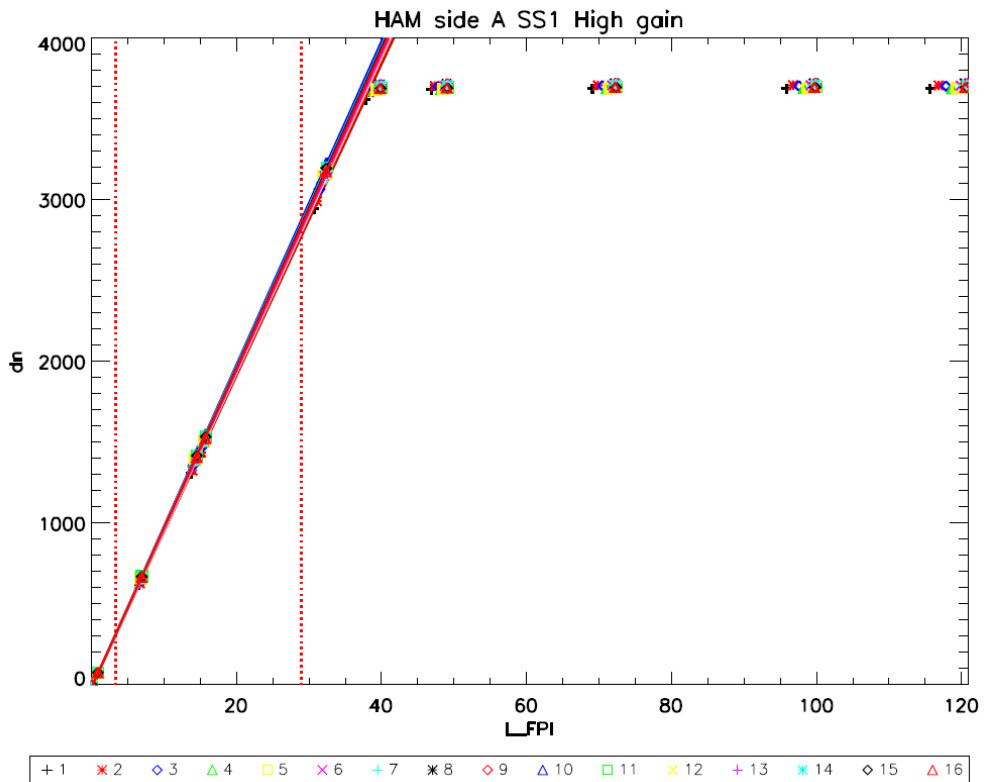


Figure 9: Fit of radiance to SNR for M1 high gain, HAM side A (using December 2014 data).

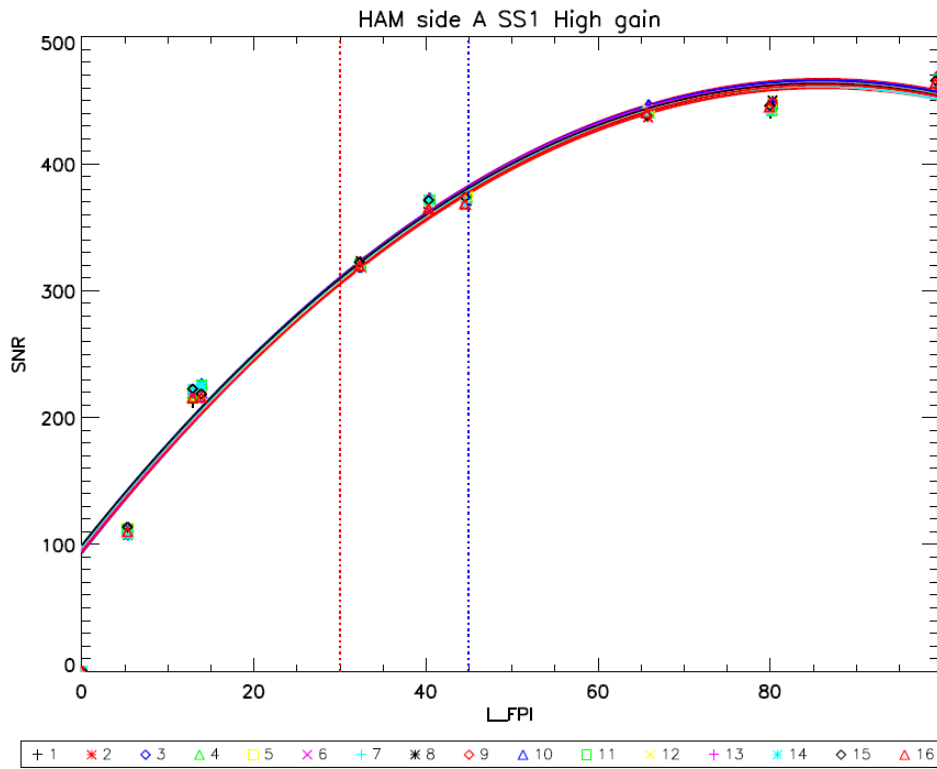


Figure 10: Fit of radiance to SNR for M7 high gain, HAM side A (using December 2014 data).

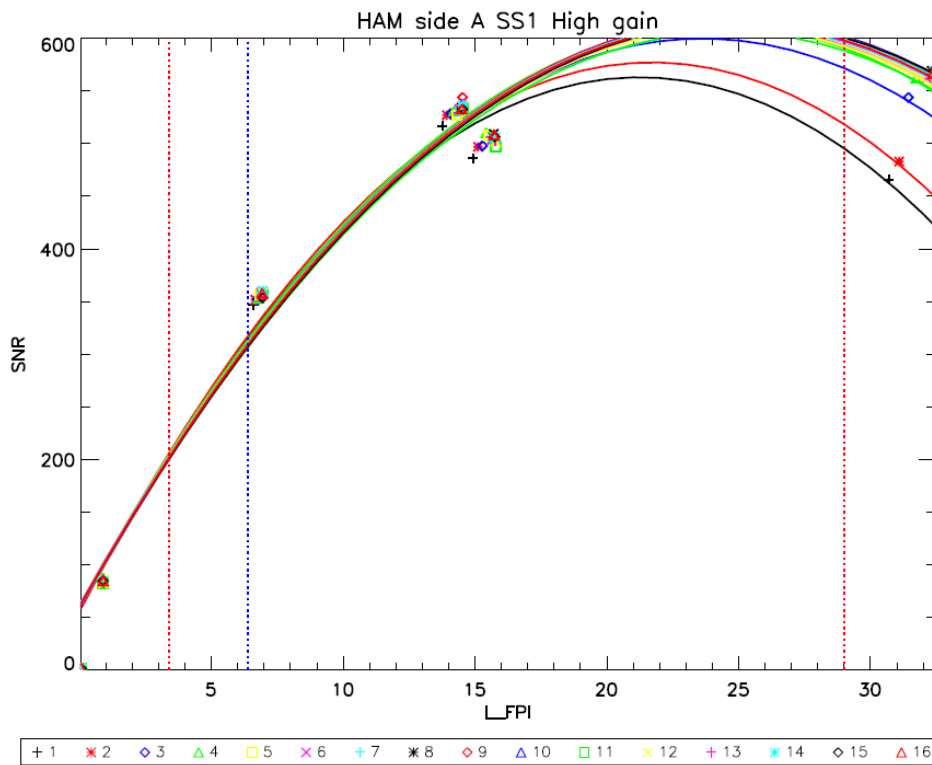


Figure 11: Example of temporal and spatial variations observed in March 2015 FPI testing. Band M1 high gain, detector 6, HAM A is shown for scans 1, 19, 39, 59, 79, and 99 (the FPI at 100 %).

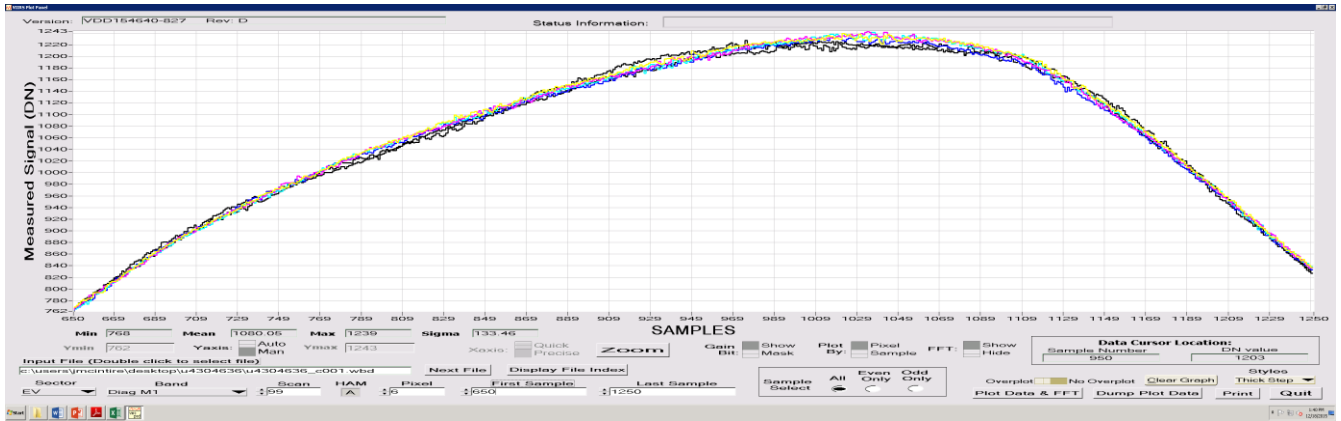


Figure 12: Band M1, scan 1 dn profile for the 100 % FPI power level with fit (upper plot) and residual to fit (lower plot), from March 2015 data.

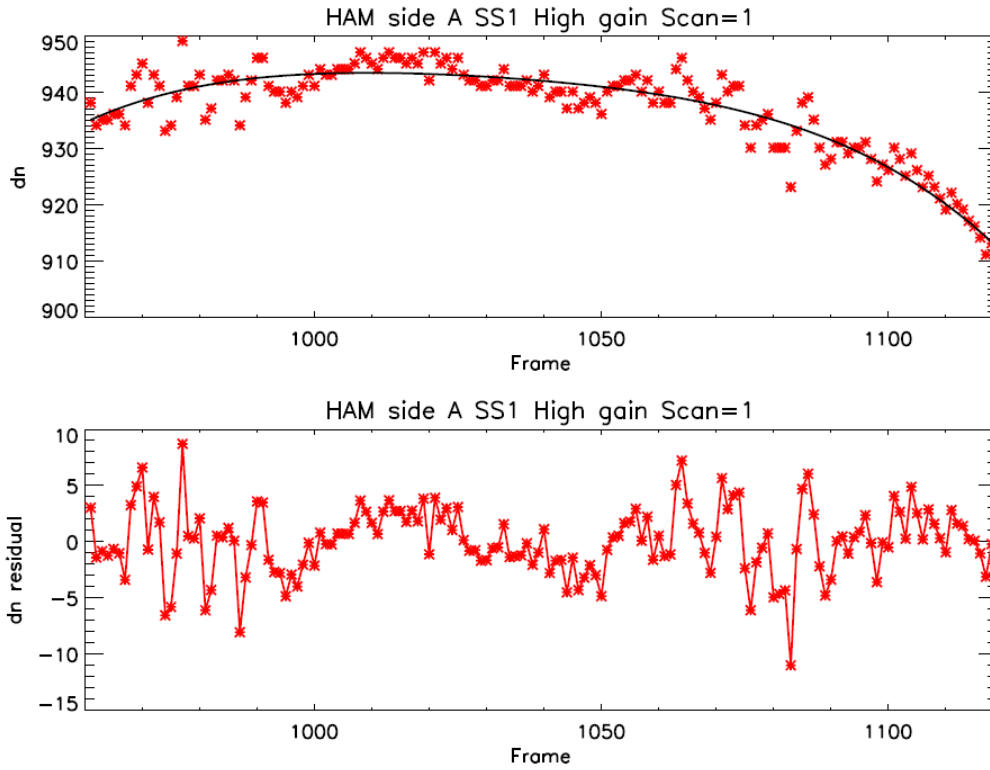


Figure 13: Band M1, scan 31 dn profile for the 100 % FPI power level with fit (upper plot) and residual to fit (lower plot), from March 2015 data.

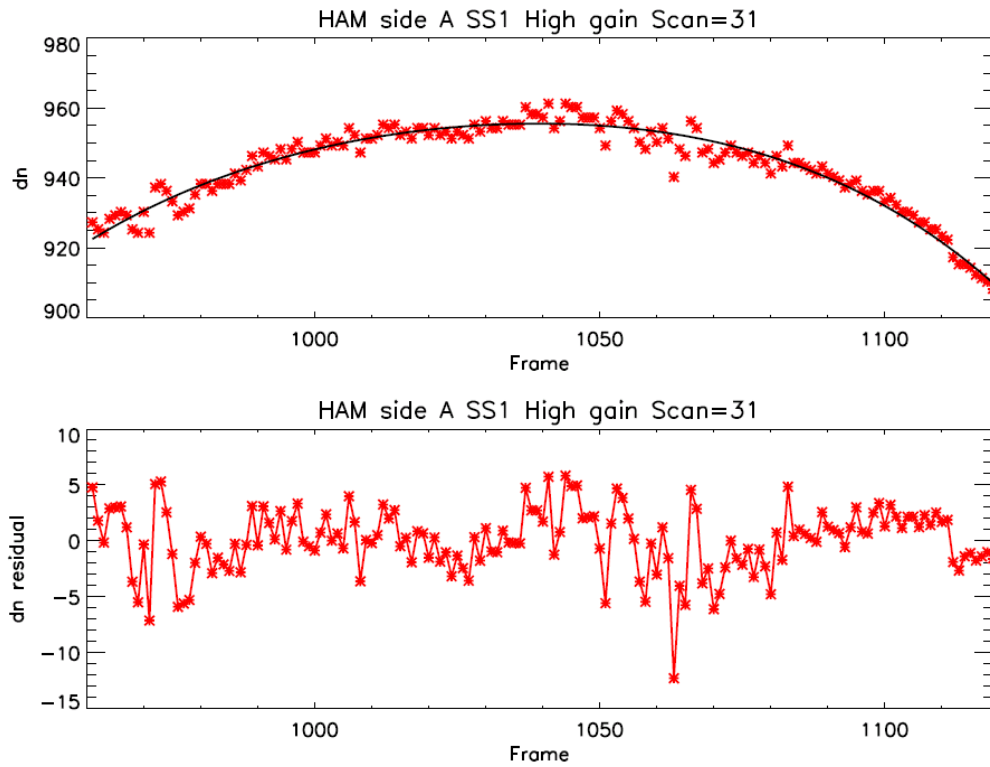


Figure 14: Fit of radiance to dn for M1 high gain, HAM side A (using March 2015 data).

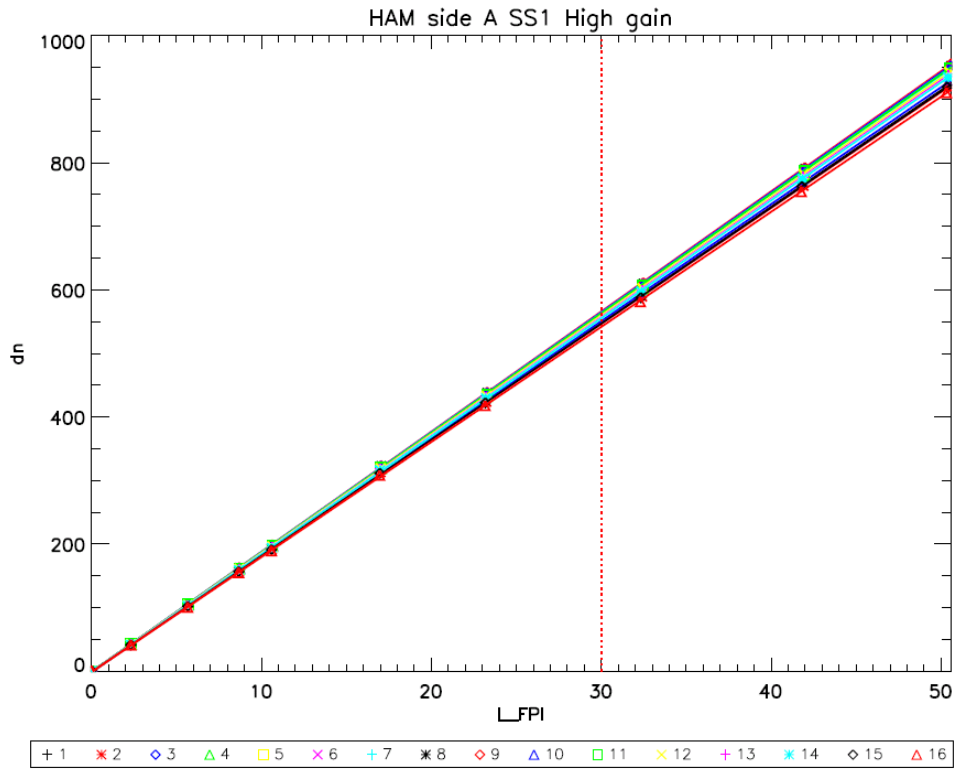


Figure 15: Fit of radiance to dn for M7 high gain, HAM side A (using March 2015 data).

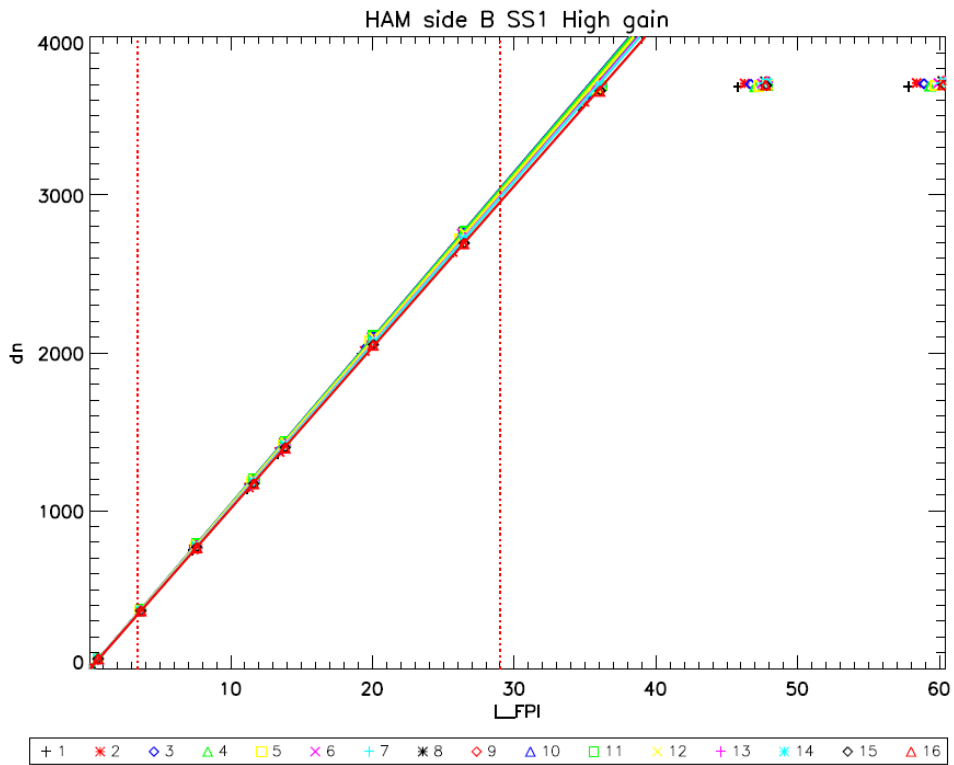


Figure 16: Fit of radiance to SNR for M1 high gain, HAM side A (using March 2015 data).

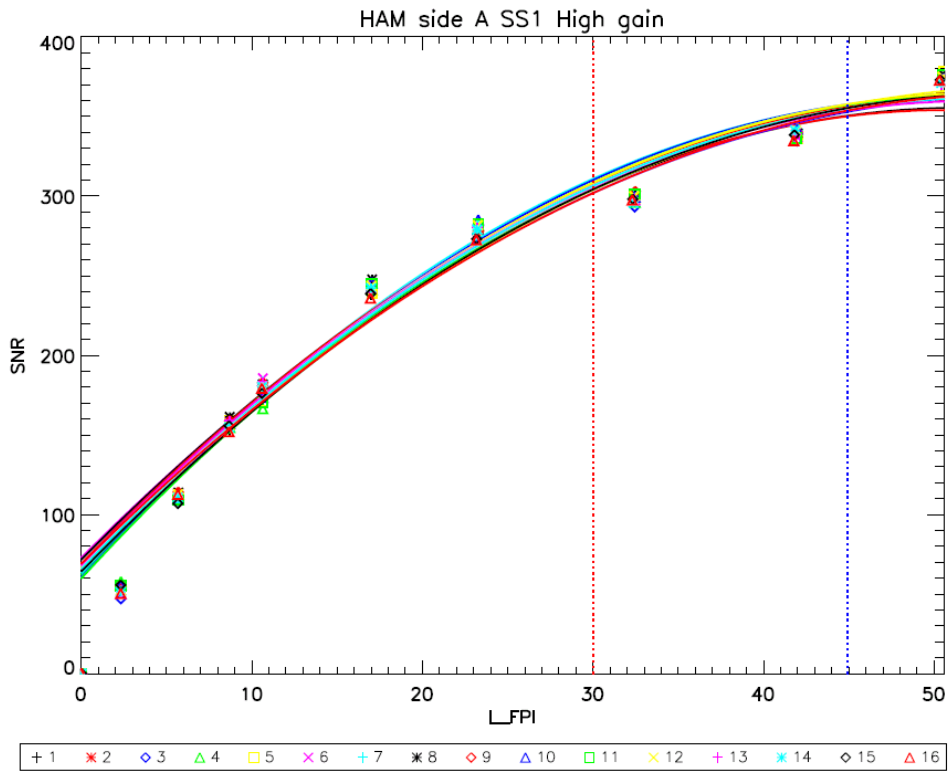


Figure 17: Fit of radiance to SNR for M7 high gain, HAM side A (using March 2015 data).

